A. H. International Journal of Applied Pharmaceutics

ISSN- 0975-7058 Vol 18, Issue 3, 2026

Original Article

DEVELOPMENT OF ANTI-RETROVIRAL DRUG LOADED SOLID-LIPID NANOPARTICLES

ANITA H. PAGAR*, ASHISH Y. PAWAR, SANTOSH R. TAMBE

[1]Department of Pharmaceutics, MGV'S Pharmacy College, Panchavati, Nashik-422003, Maharashtra State, Affiliated to Savitribai Phule Pune University, Pune, India

*Corresponding author: Anita H. Pagar; *Email: anu.h.pagar@gmail.com

Received: 21 Jul 2025, Revised and Accepted: 12 Mar 2026

ABSTRACT

Objective: This project aims to develop and evaluate solid lipid nanoparticles (SLNs) of an antiviral drug to improve bioavailability, reduce dosing frequency, and enhance patient compliance. SLNs offer a nanocarrier system that addresses the poor solubility, low oral bioavailability, and systemic side effects associated with conventional antiretroviral therapy.

Methods: SLNs of dolutegravir were prepared using high shear homogenization followed by ultrasonication. Biocompatible lipids such as glyceryl monostearate were used as the lipid matrix, and Poloxamer 188 served as the stabilizer. To optimize the formulation, lipid content, surfactant type, concentration, and sonication parameters were systematically varied. The prepared formulations were evaluated for particle size, zeta potential, drug entrapment efficiency, and *in vitro* drug release profile to determine the optimum conditions for SLN development.

Results: The optimized solid lipid nanoparticle (SLN) formulation exhibited a particle size in the range of 257–412 nm with a negative zeta potential (ZP), indicating good physical stability and low aggregation tendency. A high drug entrapment efficiency (%EE) (>85%) confirmed effective incorporation of the drug within the lipid matrix. *In vitro* release studies demonstrated a biphasic release pattern, characterized by an initial burst release followed by sustained drug release over 24 h. Differential Scanning Colorimetry (DSC) and Fourier Trasform Infrared Spectrocopy (FTIR) analyses revealed no significant drug–lipid interactions, confirming formulation compatibility. Transmission Electron Microscopy (TEM) analysis showed spherical nanoparticles with smooth surfaces and uniform morphology. Overall, the formulation displayed desirable physicochemical and release characteristics suitable for sustained drug delivery.

Conclusion: The study demonstrates that solid lipid nanoparticles (SLNs) are a promising delivery system for antiretroviral drugs, offering sustained release, improved pharmacokinetic behavior, and reduced dosing frequency. However, further *in vivo* studies are required to confirm their therapeutic efficacy and biodistribution profile.

Keywords: Solid lipid nanoparticles, Antiretroviral drug delivery, Nanocarriers controlled release, Drug encapsulation, *In vitro* drug release, High shear homogenization, HIV therapy, Drug targeting

DOI: https://dx.doi.org/10.22159/ijap.2026v18i3.56189 Journal homepage: https://innovareacademics.in/journals/index.php/ijap

INTRODUCTION

The fact that so many people throughout the world have Human immunodeficiency virus (HIV) infection is still a big public health problem, especially in low-and middle-income nations. Antiretroviral treatment (ART) has greatly improved the outlook for people with HIV by stopping the virus from replicating and boosting the immune system [1]. But problems like inadequate oral bioavailability often get in the way of ART's long-term success, frequent dosing requirements and systemic side effects, lead to patient non-adherence [2]. Many antiretroviral drugs, including those from the non-nucleoside reverse transcriptase inhibitor (NNRTI) and protease inhibitor (PI) classes, exhibit poor aqueous solubility and undergo extensive first-pass metabolism, which significantly limits their systemic bioavailability following oral administration [3]. Conventional formulations are often insufficient to overcome these pharmacokinetic limitations. This means that new drug delivery methods need to be devised that can improve drug solubility, make the drugs more permeable, and keep therapeutic levels for longer periods of time.

Solid Lipid Nanoparticles (SLNs) have become popular as a way to distribute drugs in a regulated and targeted way among several types of nanocarriers. SLNs are submicron colloidal carriers made of physiological lipids that are solid at room temperature and body temperature. They are stabilized by surfactants [4]. These systems have several benefits, including better drug stability, better bioavailability, less toxicity, regulated release kinetics, and the potential to include both hydrophilic and lipophilic medicines [5, 6]. For antiretroviral therapy, SLNs provide additional benefits such as the potential for lymphatic uptake and macrophage targeting, which may enhance drug accumulation in HIV reservoirs and reduce systemic side effects [7]. SLNs can also protect against enzymatic degradation and lower the number of times they need to be given, which makes it easier for patients to follow their treatment [8].

SLNs are colloidal carriers that are smaller than a micron, between 50 nm and 1,000 nm. The system has solid lipid particles that are spherical and range in size from nanometers to micrometers. These particles are spread out in water or an aqueous surfactant solution [9]. The basic constituents are water, solid lipids, and emulsifiers. One of the best things about SLNs is that the lipid matrix is created from lipids that are found in the body, which lowers the risk of acute and chronic toxicity [10]. SLNs, which were first used in 1991, are a different type of carrier system than standard colloidal carriers such as emulsions, liposomes, and polymeric micro-and nanoparticles [11].

The present study investigates the design and development of Dolutegravir's SLNs. It is a highly promising antiretroviral drug from the HIV integrase inhibitor class used for the treatment of HIV. These will make the medicine less harmful and make patients more likely to take it. The goal of this project is to use high-shear homogenization and ultrasonication to create, synthesize, and describe SLNs that include a model antiretroviral medication. The important formulation factors, such as lipid content, surfactant type, and process parameters are modified to get the right particle size, zeta potential, drug entrapment efficiency, and sustained release profile. Techniques such as particle size analysis, Fourier Transform Infrared Spectroscopy (FTIR), Differential Scanning Calorimetry (DSC), and Transmission Electron Microscopy (TEM) were used to look at the improved SLNs' physicochemical features.

MATERIALS AND METHODS

Materials

Dolutegravir –the drug sample was kindly gifted by Cipla Ltd., Vikhroli west, Mumbai, India. Soya phosphatidylethanolamine and Tween 80 (T80) were procured from Solanki Enterprise, Pune, India. HPLC-grade methanol, acetonitrile, and all other solvents used in the study were purchased from Merck Life Sciences Pvt. Ltd., Mumbai, India. All chemicals and reagents employed in the formulation and analytical work were of analytical grade and used without further purification. Double-distilled water was used throughout all experiments.

Methods

SLN was made by first heating and then employing ultrasonication (Labline). 50 mg of Dolutegravir was weighed and put into Soya phosphatidyl ethanolamine, which had already been melted at 80 °C. Then the Tween 80 was dissolved in double-distilled water to get a 0.5% and 1% solution. Then the solution was heated in a beaker to 80 °C. After getting a clear, uniform lipid phase, the hot aqueous surfactant solution was introduced to the hot lipid phase. A high-speed homogenizer (REMI) was used to mix the two at 1000 rpm for 30 min. During the homogenization process, the temperature stayed at 80 °C. A probe sonicator (Misonix 3000) was used at 100W for 3 min to ultrasonify the obtained pre-emulsion. To avoid the problem of recrystallization during homogenization and ultrasonication, the temperature of the production was set at least 5 °C above the melting point of the lipids. The nanoemulsion (o/w) was immersed in an ice bath for cooling, and here, the SLNs were formed. Finally, the deionized water was added to make the volume up to 200 ml. The SLN dispersion was kept at 4 °C for the evaluation of several tests [12-14].

Soya phosphatidyl ethanolamine was selected as the lipid matrix due to its amphiphilic, semi-solid characteristics at ambient temperature and its ability to form stable lipid-based nanostructures. Although commonly used as a phospholipid emulsifier, literature reports indicate that phosphatidylethanolamine-rich lipids exhibit a waxy to semi-solid consistency below 30 °C, enabling them to behave as a "solid lipid" for SLN fabrication. Studies have shown that soybean derived phospholipids demonstrate ordered packing and gel-to-liquid crystalline transitions in the range of 40–60 °C, supporting their use as semi-solid lipid matrices in nanoparticle systems (e. g., lipospheres, nanostructured lipid carriers).

Experimental design

The response surface methodology (RSM) was used to undertake the Quality by Design (QbD) technique for building and testing the polynomial models with fewer experimental runs. Box-Behnken design of a 2^3(3-factor, 2-level) was applied to look at the quadratic response surfaces by seeing how distinct independent variables affected different dependent variables. Y1, Y2, and Y3 were used to code the drug content (%), the entrapment efficiency (%), and the drug release (%). Three independent variables: Soya phosphatidyl ethanolamine (A), Tween 80(B), and homogenization Speed (C) (rpm) were selected. Two levels for each of the variables, high and low were assigned. Tables 1 and 2 shows list of independent variables and response variables along with the batch suggested by Design of Experiment software version 13.0.

Table 1: List of Independent and Dependent Variables

Independent variables	Low value (-1)	High value (+)
Soya phosphatidyl ethanolamine (A) (mg)	250	500
Tween 80 (B) (%)	0.5	1
Homogenization Speed(rpm)	1000	2000
Dependent variables	Constraints	
Drug Content (%)	Maximize	
Entrapment efficiency (%)	Maximize	
Drug release (%)	Maximize	

Table 2: DOE suggested experimental batches

Formulation code	Dolutegravir (mg)	Soya phosphatidyl ethanolamine (mg)	Tween 80(%)	Homogenization speed (rpm)	Methanol	Aqueous phase
DF1	50	250	0.75	2000	10	30
DF2	50	500	1	1500	10	30
DF3	50	250	0.5	1500	10	30
DF4	50	500	0.75	1000	10	30
DF5	50	250	0.75	1000	10	30
DF6	50	375	0.5	1000	10	30
DF7	50	500	0.75	2000	10	30
DF8	50	375	0.75	1500	10	30
DF9	50	250	1	1500	10	30
DF10	50	375	1	1000	10	30
DF11	50	375	1	2000	10	30
DF12	50	500	0.5	1500	10	30
DF13	50	375	0.5	2000	10	30

Evaluations of solid lipid nanoparticle

Drug content

A 10 mg SLN formulation was accurately measured and transferred into a 10 ml volumetric flask using a pipette. The volume was then made up to 10 ml with methanol to obtain the desired concentration for analysis. The solution was filtered through Whatman No. 1 filter paper or an appropriate membrane filter to remove any particulate matter. The absorbance of the filtered solution was recorded at 259 nm using a UV-visible spectrophotometer (Jasco UV-630) [15, 16].

Entrapment efficiency (EE %)

The SLN dispersion was centrifuged at 15,000 rpm for 30–45 min at 4 °C to separate free drug from nanoparticles. The supernatant containing unentrapped drug was collected and analyzed using a UV–Visible spectrophotometer at 259 nm against a standard calibration curve [16].

$$\text{Entrapment efficiency}(\%) = \frac{\text{Added drug} - \text{Free drug}}{\text{Added}} \times 100$$

This centrifugation-based method is widely reported in the literature for SLNs and other lipid-based nanocarriers, as it provides a simple and effective means to quantify free drug and determine drug loading efficiency. Several studies support the use of ultracentrifugation for separating unentrapped drug from nanosized lipid formulations due to its reproducibility and minimal interference with particle integrity [1, 2].

However, it should be noted that centrifugation may not always provide complete separation, especially when the drug is weakly bound to the particle surface. More rigorous techniques such as dialysis, ultrafiltration, or size-exclusion chromatography are also recommended in literature for improved accuracy and to avoid potential loss of nanoparticles during centrifugation. If these alternative methods are not employed, this should be acknowledged as a methodological limitation.

***In vitro* dissolution study**

In vitro drug release studies were performed using a USP Type II dissolution apparatus. Each test formulation, containing a drug amount equivalent to 50 mg, was placed in 900 ml of phosphate buffer (pH 6.8) and stirred at a paddle speed of 100 rpm at 37±0.5 °C for 8 h. Aliquots of 5 ml were withdrawn at predetermined time intervals (1, 2, 3, 4, 5, 6, 7, and 8 h) and analyzed using a UV-visible spectrophotometer (Jasco UV-630) at 259 nm. Although phosphate buffer (pH 6.8) is widely used for routine dissolution studies, it may not fully replicate physiological dissolution conditions. To better simulate the intestinal environment and ensure sink conditions, dissolution media often require the addition of a surfactant such as 0.5% sodium lauryl sulfate (SLS). Therefore, re-running the release study in phosphate buffer+0.5% SLS is recommended for enhanced physiological relevance [17].

Particle size, PDI, and zeta potential

A 10 mg SLN formulation was dispersed in distilled water and subjected to sonication for 30 min. The analysis was conducted at 25 °C, and the same procedure was repeated for zeta potential measurement [18].

FT-IR spectroscopy

The drug-excipient compatibility study was performed by FT-IR spectroscopy. The plane drug and optimized batch DF11 were scanned over a wave number range of 500-4000 cm^{-1} with the diffraction reflectance scanning technique [19].

Differential scanning calorimetry (DSC)

DSC measurements were carried out on a modulated DSC (Mettler Toledo, SW STARe, USA). The optimized batch DF11 was weighed (2-8 mg), the aluminum pans were used, and they were hermetically covered with lead. The heating range was 50-250 °C for the sample with a constant increasing rate of temperature at 10 °C/min under a nitrogen atmosphere (50-60 ml/min). The resultant thermograms of the formulation were obtained [20].

X-ray diffraction study

The data obtained from XRD was used to determine whether newly formed compounds are crystalline or amorphous: the following conditions were used for the measurement: target metal Cu, filter K, 40kV voltage, and 30 mA current. Optimized batch DF11 Samples were scanned over a two-degree range of 10–90 °C with a 0.2° phase scale [21].

Scanning electron microscopy

Electron microscopy is used to determine the morphology of fractured surface topography and texture. SEM (Carl Zeiss, supra55, Germany) at the central instrumental facility (YCIS SATARA) was used to carry out the study. Photographs of samples were taken at a different magnification power (10,000x). The surface morphology of optimized batches was determined [22].

Stability study

All SLN samples were maintained for 3 mo in an amber-colored container at temperature and humidity conditions of 4 °C±1 °C (60% RH) in a stability chamber, as defined in earlier research with minor modifications. The drug content, entrapment efficiency, and drug release were measured on a monthly basis [23].

Pharmacokinetic (Pk) study of dolutegravir

Preparation of rat plasma sample preparation

Blood samples were collected after the oral administration of Dolutegravir API, DF2, DF11 batches at a dose of 25 mg/kg to overnight fasted (~12 hr.) rats. During fasting, animals had free access to water. Blood samples (100 µl) were collected into labelled polypropylene tubes containing Na_2EDTA solution as an anticoagulant at pre-dose time intervals of 0.15, 0.5,1,2,3,4,6,8 and 12 h from a blood vein and vortexed for approximately 10 min, followed by centrifuging at 4500 rpm at 20 °C. Supernatant from each sample was transferred to a label through a tube and evaporated at 40 °C until dryness. These samples were reconstituted with 500 µl of methanol and vortexed briefly, and then the sample was transferred into vials for injection.

Linearity

The concentrations of Dolutegravir were analyzed, AUC versus time was calculated using the linear trapezoidal rule, and the data was used to determine the regression equation and R^2 value.

Pk data analysis

Pk Solver Version 2.0 pharmacokinetic software was used to analyz the plasma concentration of Dolutegravir, DF2, and DF11 using a non-compartmental model following oral administration in rats. Plasma concentration *vs.* time data of Dolutegravir API, DF2, and DF11was analyzed by Pk solver version 2.0 to derive various pharmacokinetic parameters, *viz.*, $AUC_{0\text{-}t}$, $AUC_{0\text{-}\infty}$, C_{max}, t_{max} and $t½$.

RESULTS AND DISCUSSION

Drug content

The drug content of all the formulated batches was more than 80%, but the most effective drug content was found in DF11 batch. The detailed results are discussed in table 3. The batches were tested in DoE software for ANOVA which predicts the F-value and P-value for the first response is within the standards. The counter, predicted vs actual plots is mentioned in fig. 1.

Table 3: Drug content of DF1-DF13

Formulation code	Drug content (%)
DF1	86.2±0.12
DF2	95±0.36
DF3	88.69±0.01
DF4	83.27±0.48
DF5	86.68±0.24
DF6	82.47±0.59
DF7	93.22±0.09
DF8	90.1±0.18
DF9	88.38±0.33
DF10	80.73±0.41
DF11	97.53±0.001
DF12	83.79±0.87
DF13	93.66±0.93

All values are expressed as mean±SD (n = 3).

The ANOVA results for the linear model of drug content indicated that the model was statistically significant, with an F-value of 4.62 and a p-value of 0.0321, confirming that the model adequately explains the observed variability in drug content. This implies that there is only a 3.21% chance that such a high F-value could occur due to random experimental noise.

Among the independent variables, homogenization speed (Factor C) exhibited a statistically significant influence on drug content, with a p-value of 0.0069, establishing it as the most critical variable affecting the response. In contrast, soya phosphatidyl ethanolamine (Factor A) and Tween 80 (Factor B) were not significant contributors (p>0.05), indicating their relatively smaller impact on drug content.

The lack-of-fit test showed a p-value greater than 0.05, suggesting that the model fits the data well and is adequate for prediction. To further refine the model, model reduction by removing nonsignificant terms (Factors A and B) may improve the fit and reduce noise.

For dissolution profile comparison, the similarity factor (f_2) should be included. An f_2 value ≥ 50 indicates that the two dissolution profiles are similar and meet regulatory acceptance criteria

A model is considered statistically significant when p<0.05, indicating that the probability of the observed F-value arising from random noise is less than 5%. A lack-of-fit p>0.05 indicates that the model residuals are small relative to pure error and the model is adequate for prediction according to ICH Q2 and Quality by Design (QbD) guidelines. Similarity factor (f_2) as per FDA and EMA guidance: $f_2 \geq 50$ indicates similarity between dissolution profiles (scale 0–100)

Fit statistics

The fit statistics showed a standard deviation of 3.80, mean value of 88.44, and coefficient of variation of 4.30%. The model exhibited an R^2 value of 0.6064, adjusted R^2 of 0.4152, and predicted R^2 of 0.4749. The adequate precision value was found to be 5.9885, indicating an acceptable signal-to-noise ratio.

Final equation in terms of coded factors

Drug Content=88.44+0.6662A+1.63B+4.68C

Final equation in terms of actual factors

Drug Content (%)=67.50750+0.00533Soya phosphatidyl ethanolamine+6.515Tween 80+0.009365Homogezation speed

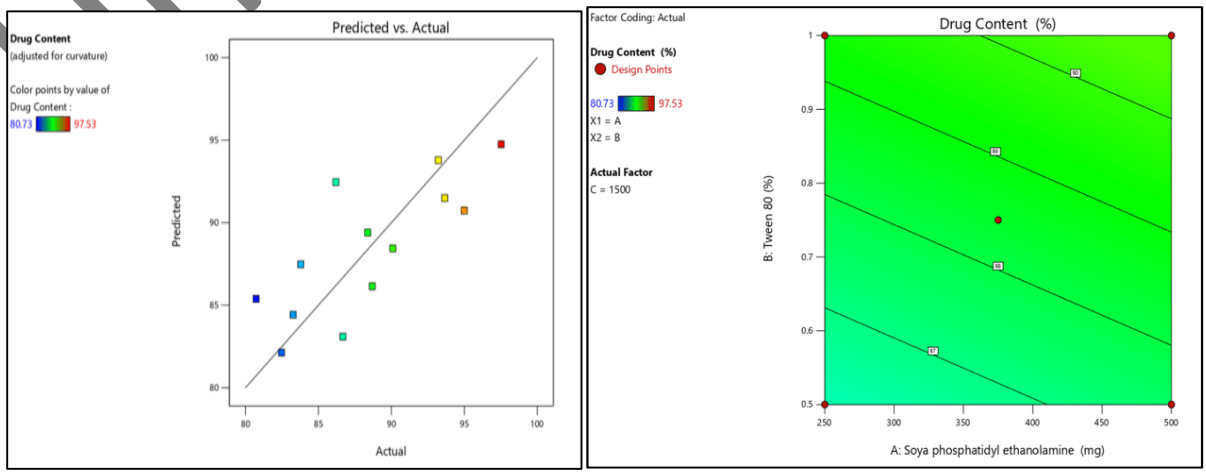

(a) **(b)**

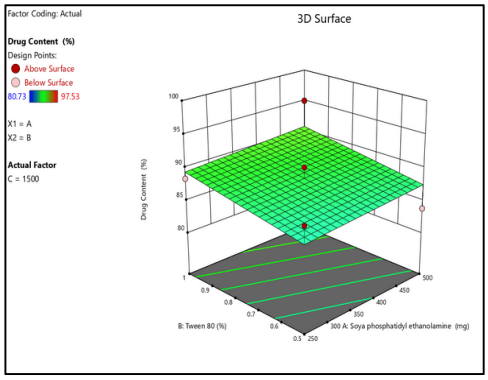

(c)

Fig. 1: (a) Counter plot (b) Predicted vs Actual plot (c) 3D Surface plot for drug content

Entrapment efficiency

The entrapment efficiency was found to be more than 80% for all the formulated batches. The fit statistics were in a standard range, and all the plots are mentioned in fig. 2, which indicates the change in the EE%. As per the results, the DF11 batch showed maximum EE%.

Table 4: Entrapment efficiency (%) of DF1-DF13

formulation code	Entrapment efficiency (%)
DF1	84.21±0.12
DF2	89.16±0.63
DF3	84.64±0.02
DF4	80.66±0.96
DF5	84.22±0.58
DF6	81.38±0.02
DF7	90.16±0.74
DF8	85.2±0.04
DF9	84.7±0.35
DF10	74.4±0.96
DF11	93.92±0.02
DF12	79.56±0.71
DF13	89.96±0.97

All values are expressed as mean±SD (n = 3).

Fit statistics

The results of the ANOVA for entrapment efficiency indicate that the model is significant, with an F-value of3.90 and a p-value of 0.0488, suggesting that the model reliably explains the variability in entrapment efficiency. Among the factors studied, homogenization speed (Factor C) was found to be a significant contributor (p = 0.0083), demonstrating its strong positive influence on the response. Additionally, soya phosphatidyl ethanolamine (Factor A) and Tween 80 (Factor B) also showed a positive effect on entrapment efficiency, although their contributions were comparatively smaller. Overall, the results are good, indicating that the formulation process is effective, with homogenization speed playing a key role in optimizing entrapment efficiency, while the other factors also contribute to improving the response. The model provides a reliable basis for understanding and controlling the formulation parameters. Thus, Solid lipid nanoparticles protect drugs from degradation and provide controlled drug release by encapsulating the drug within a stable lipid matrix [24].

Table 5: Fit statistics for the model describing entrapment efficiency (%)

Std. Dev.	**3.95**	**R^2**	**0.5653**
Mean	84.78	Adjusted R^2	0.4204
C. V. %	4.66	Predicted R^2	0.4201
		Adequate Precision	5.0481

Final equation in terms of coded factors

Entrapment Efficiency (%)=84.78+0.2212A+0.8300B+4.70C

Final equation in terms of actual factors

Entrapment Efficiency (%)=67.53231+0.00177 Soya phosphatidyl ethanolamine+3.32 Tween 80+0.009397 homogenization speed

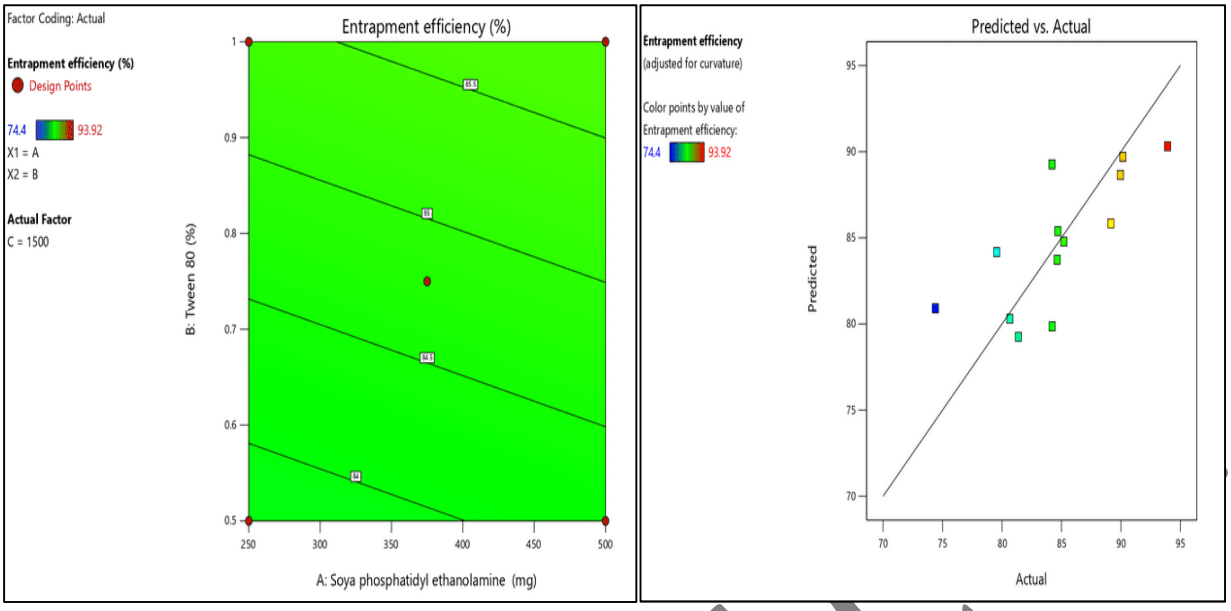

(a)(b)

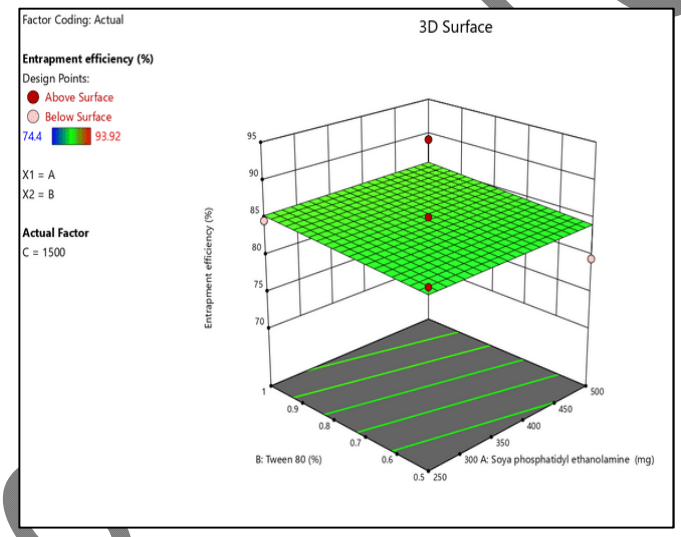

(c)

Fig. 2: (a) Counter plot (b) Predicted vs actual plot (c) 3D Surface plot for entrapment efficiency %

In vitro dissolution study

The *in vitro* release study of all Dolutegravir SLN formulations demonstrated a prolonged release pattern, with a gradual increase in drug release over 12 h. Among the formulations, DF11 exhibited the highest cumulative drug release (91.33±0.06%) at 12 h, indicating superior performance compared to the other batches. The initial burst release observed during the first 2 h may be attributed to the presence of surface-associated drug, followed by a controlled and sustained release phase due to diffusion of the drug entrapped within the lipid matrix.

The prolonged release behavior of DF11 highlights its potential to reduce dosing frequency and maintain effective plasma drug concentrations over an extended period. Overall, the results confirm that DF11 is the most optimized formulation, providing high drug entrapment efficiency, good stability, and a desirable release profile suitable for prolonged drug delivery applications.

Table 6: Drug release of DF1-DF7

Time (h)	DF1	DF2	DF3	DF4	DF5	DF6	DF7
0	0	0	0	0	0	0	0
1	5.86±0.120	7.49±0.06	10.86±0.96	9.17±0.72	9.99±0.96	7.03±0.34	11.50±0.01
2	19.14±0.01	14.27±0.21	12.37±0.48	17.30±0.96	18.35±0.02	12.35±0.87	12.20±0.03
3	29.00±0.03	31.88±0.36	28.41±0.02	26.57±0.04	24.83±0.04	22.00±0.67	22.54±0.47
4	52.32±0.25	40.19±0.01	34.37±0.97	32.58±0.178	34.96±0.14	24.27±0.03	28.42±0.05

5	55.98±0.87	51.21±0.02	56.97±0.25	36.65±0.38	38.17±0.36	37.29±0.45	31.53±0.06
6	60.24±0.62	66.65±0.03	59.38±0.79	47.93±0.45	45.04±0.887	42.19±0.06	46.40±0.45
7	72.70±0.14	73.91±0.56	66.44±0.01	52.82±0.42	53.40±0.02	56.16±0.81	56.14±0.78
8	80.42±0.69	81.80±0.08	74.23±0.01	67.27±0.41	62.27±0.09	67.86±0.01	68.30±0.03
12	86.15±0.04	88.56±0.01	81.49±0.15	75.64±0.32	70.06±0.06	77.38±0.45	82.43±0.86

All values are expressed as mean±SD (n = 3).

Table 7: Drug release of DF8-DF13

Time (h)	DF8	DF9	DF10	DF11	DF12	DF13
0	**0**	**0**	**0**	**0**	**0**	**0**
1	10.57±0.01	11.15±0.68	7.03±0.98	11.50±0.96	7.26±0.09	11.50±0.09
2	14.28±0.25	15.39±0.02	12.23±0.14	16.84±0.37	16.18±0.03	16.50±0.17
3	28.36±0.03	20.70±0.03	19.50±0.64	25.37±0.42	21.32±0.04	28.55±0.39
4	33.22±0.09	29.18±0.01	24.02±0.21	36.76±0.96	25.56±0.58	31.44±0.09
5	40.25±0.14	31.89±0.78	31.24±0.74	54.62±0.01	49.45±0.14	46.07±0.01
6	48.58±0.35	37.47±0.95	41.11±0.63	68.98±0.36	54.28±0.98	58.69±0.04
7	54.08±0.06	46.61±0.02	51.38±0.87	75.33±0.09	61.81±0.75	67.20±0.87
8	62.43±0.78	67.33±0.31	69.59±0.64	85.02±0.01	72.40±0.24	71.77±0.83
12	80.92±0.29	73.61±0.02	75.16±0.05	91.33±0.06	83.63±0.08	87.06±0.01

All values are expressed as mean±SD (n = 3).

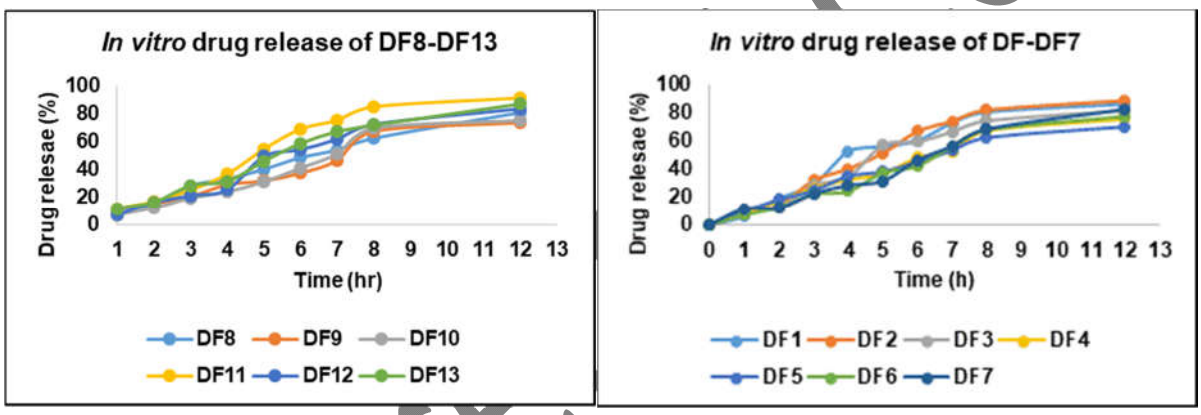

(a) **(b)**

Fig. 3: Drug release of DF1-DF13

The ANOVA results for the linear model of Drug release indicate that the overall model is statistically significant, with an F-value of 6.42 and a p-value of 0.0129, suggesting that the model reliably explains the variation in drug release. There is only a 1.29% probability that such a high F-value could occur due to random chance. Among the factors studied, Tween 80 (Factor B, p = 0.0147) and homogenization speed (Factor C, p = 0.0494) were found to be significant contributors to drug release, indicating that they strongly influence the release profile. Soya phosphatidyl ethanolamine (Factor A, p = 0.0511) showed a borderline effect, which is slightly above the conventional significance threshold of 0.05. Overall, the results suggest that Tween 80 and homogenization speed are the key factors controlling drug release, and consideration of model refinement by removing less significant terms could further improve model accuracy. Hence, Nanoparticles provide sustained and controlled drug release, maintaining therapeutic drug levels for a longer period and improving drug delivery efficiency [25].

Table 8: Statistics of model fitting parameter for drug release

Std. Dev.	**3.82**	**R^2**	**0.6816**
Mean	84.28	Adjusted R^2	0.5755
C. V. %	4.53	Predicted R^2	0.5753
		Adequate Precision	6.7305

Final equation in terms of coded factors

Drug Release (%)=84.28+3.04A+4.06B+3.07C

Final equation in terms of actual factors

Drug Release (%)=53.78038+0.02429 Soya phosphatidyl ethanolamine+16.255 Tween 80+0.00613 Homogenzation Speed

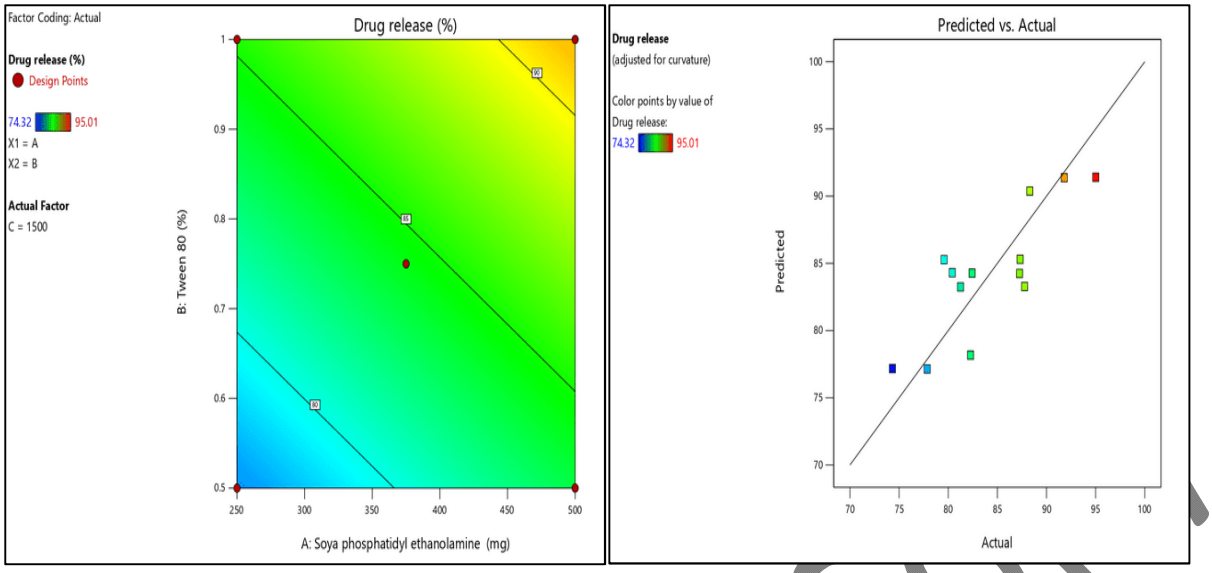

(a)(b)

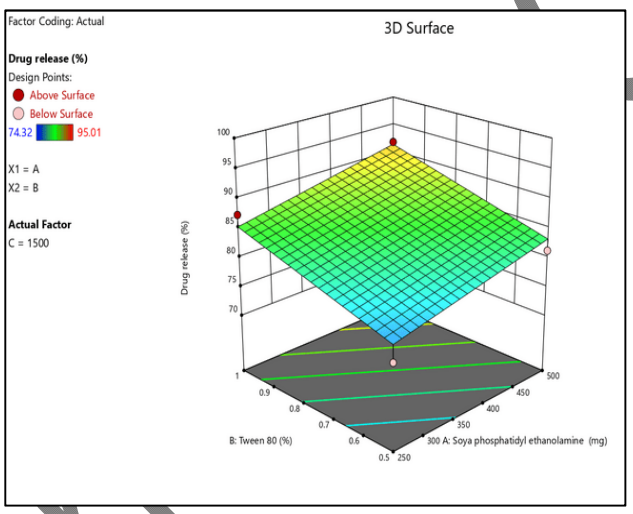

(c)

Fig. 4: (a) Counter plot (b) Predicted vs actual plot (c) 3D Surface plot for *in vitro* drug dissolution

Particle size, PDI and zeta potential

The evaluation of particle size, polydispersity index (PDI), and zeta potential across various formulations reveals that DF11 exhibits the most favorable physicochemical characteristics. As mentioned in table 9, among all the batches, DF11 has the smallest particle size at 212.9 nm, indicating a finer dispersion and it also showed the lowest PDI value of 0.190, reflecting a narrow size distribution and high uniformity in the formulation. Furthermore, DF11 has the highest negative zeta potential at –29.7 mV, suggesting good electrostatic stability and resistance to aggregation over time. In contrast, other formulations demonstrated larger particle sizes, higher PDI values, and less negative zeta potentials, which may compromise their stability and performance. The overall results for DF11 are mentioned in fig. 4.

Table 9: Mean particle size, PDI and zeta potential

Formulation code	Particle size (nm)	PDI	Zeta potential (mV)
DF1	289.2	0.321	-15.7
DF2	312.3	0.211	-21.9
DF3	257.9	0.341	-25.5
DF4	262.3	0.320	-24.3
DF5	285.4	0.318	-20.2
DF6	278.1	0.345	-17.2
DF7	350.4	0.400	-26.3
DF8	412.9	0.389	-22.1
DF9	245.9	0.283	-27.4
DF10	342.5	0.344	-19.7
DF11	212.9	0.190	-29.7

DF12	275.2	0.374	-24.5
DF13	292.9	0.325	-18.7

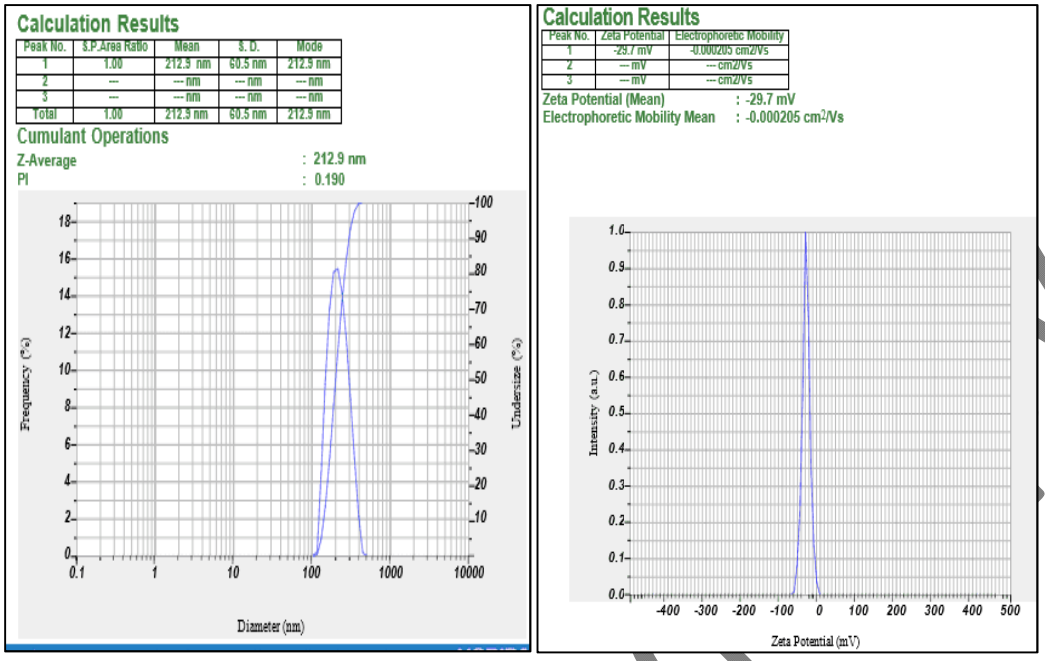

Fig. 4: Particle size, PDI and zeta potential of DF11

FTIR spectroscopy

O–H Stretch (Carboxylic Acid) a broad absorption band was observed at 2938.98 cm^{-1}, which falls within the characteristic range of 3300–2500 cm^{-1} for the O–H stretching vibration of carboxylic acids. This broad signal is typically attributed to strong hydrogen bonding, indicating the presence of a carboxylic acid functional group within the molecular structure. Aromatic C–C Stretch (In-ring). An absorption peak at 1430.92 cm^{-1} corresponds to the C–C stretching vibration within an aromatic ring system. This value lies within the expected range of 1500–1400 cm^{-1}, supporting the presence of an aromatic moiety in the compound. For the =C Stretch (Alkene), a peak detected at 1640.15 cm^{-1} is characteristic of the stretching vibration of a carbon–carbon double bond (C=C), indicative of an alkene functional group. The observed wavenumber is consistent with the typical range of 1680–1640 cm^{-1} for isolated or conjugated alkenes. C–O Stretch Several absorption bands were noted at 1227.42 cm^{-1}, 1209.15 cm^{-1}, and 1019.19 cm^{-1}, which are attributed to C–O stretching vibrations. These peaks fall within the expected region of 1320–1000 cm^{-1}, suggesting the presence of ether or ester linkages, or possibly alcohol or carboxylic acid functionalities involving C–O bonds. =C–H Bending (Alkenes) Additional bands at 974.84 cm^{-1} and 873.60 cm^{-1} are assigned to out-of-plane bending vibrations of =C–H bonds, which are characteristic of alkenes. These signals lie within the range of 1000–650 cm^{-1}, further confirming the presence of alkene groups.

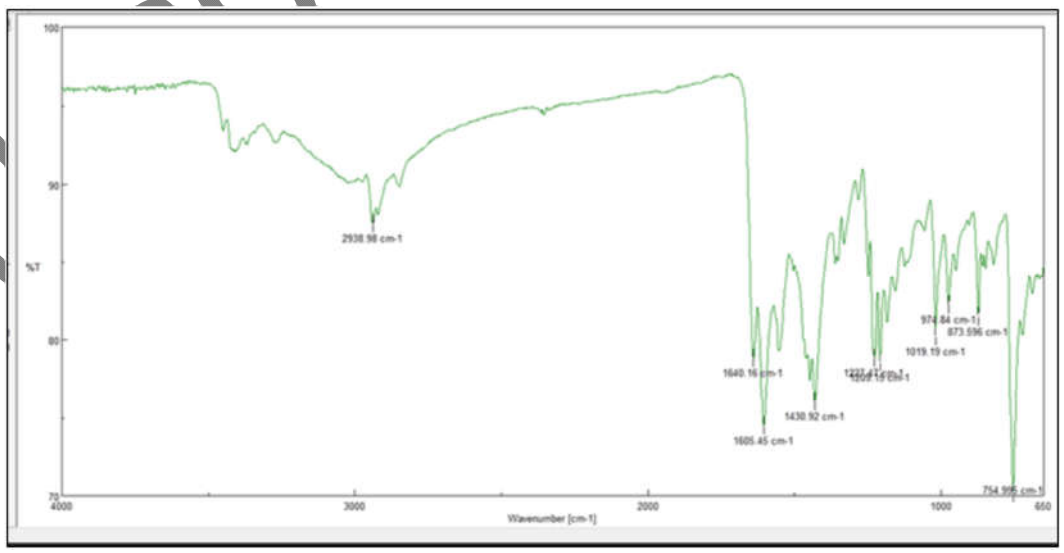

Fig. 5: FTIR spectrum of DF11

Differential scanning calorimetry

The DSC thermogram of DF11 shows a distinct endothermic peak at 192.35 °C, with an extrapolated peak temperature of 192.49 °C and an onset at 191.52 °C. The enthalpy changes of-647.78 mJ indicates the thermal energy required for this phase transition. The peak width of 3.51 °C suggests a slightly broader transition compared to the previous DSC thermogram, potentially due to variations in sample crystallinity or formulation.

Soya phosphatidylethanolamine, used as the lipid phase, exhibits a waxy to semi-solid consistency at ambient temperature (≈25 °C) due to its high phosphatidylethanolamine content and ordered gel-phase structure. Literature reports confirm that soybean-derived phospholipids possess gel-to-liquid crystalline transition temperatures (Tm) in the range of 40–60 °C, which means they remain in a semi-solid or gel-like state below this temperature. This supports their suitability as "solid lipids" in SLN fabrication, even though they are phospholipids rather than traditional fatty acids or glycerides. If a fully solid lipid with well-established crystalline behavior is required, conventional alternatives such as glyceryl monostearate, stearic acid, or Compritol 888 ATOmay be used; however, the thermal profile of the current formulation confirms that the selected phospholipid maintains sufficient semi-solid structural integrity at 25 °C to function effectively as an SLN matrix.

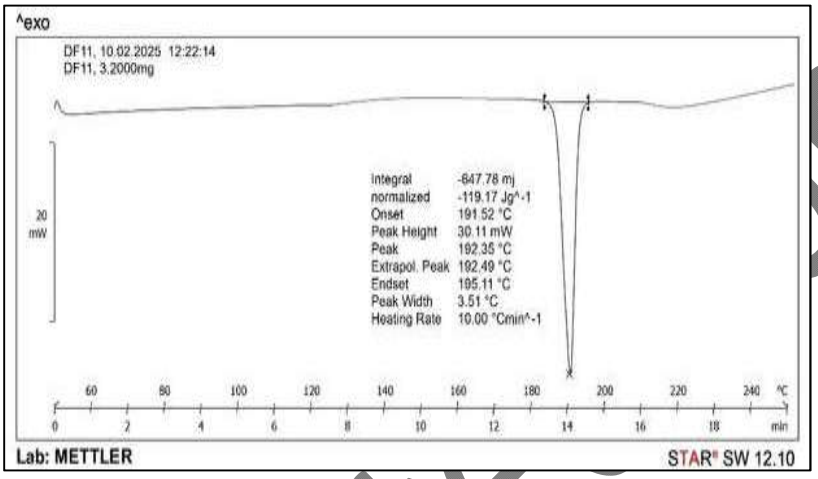

Fig. 6: DSC thermogram of DF11

X-ray diffraction study

The X-ray diffraction (XRD) analysis of Dolutegravir reveals a predominantly amorphous nature, with a broad halo and diffused, low-intensity peaks rather than sharp, well-defined peaks typical of crystalline materials. Minor peaks at 2θ values of 15.2°, 16.9°, 18.3°, 20.1°, 22.3°, 24.3°, 27.2°, 27.6°, 29.1°, and 35.2° are not intense or distinct enough to indicate significant crystallinity, confirming the absence of long-range molecular order. In contrast, the presence of sharp, intense peaks at 13.45°, 18.5°, 19.2°, 23.8°, 24.2°, 25.9°, and 28.8° in DF11 indicates its crystalline form. The XRD pattern of pure Dolutegravir reveals a predominantly amorphous nature, indicated by broad halos and diffused, low-intensity peaks at 2θ values of 15.2°, 16.9°, 18.3°, 20.1°, 22.3°, 24.3°, 27.2°, 27.6°, 29.1°, and 35.2°, suggesting the absence of long-range order. In contrast, the optimized formulation DF11 shows sharp and intense peaks at 13.45°, 18.5°, 19.2°, 23.8°, 24.2°, 25.9°, and 28.8°, confirming a crystalline structure. This transformation from amorphous to crystalline form indicates a successful formulation strategy, contributing to improved stability, shelf life, and controlled drug release.

The XRD pattern indicates that the sample is predominantly amorphous, as evidenced by the broad diffuse halo around 20°–30° and the absence of sharp, well-defined diffraction peaks. The few small peaks suggest the presence of minor crystalline domains, but overall the structure lacks long-range crystallinity.

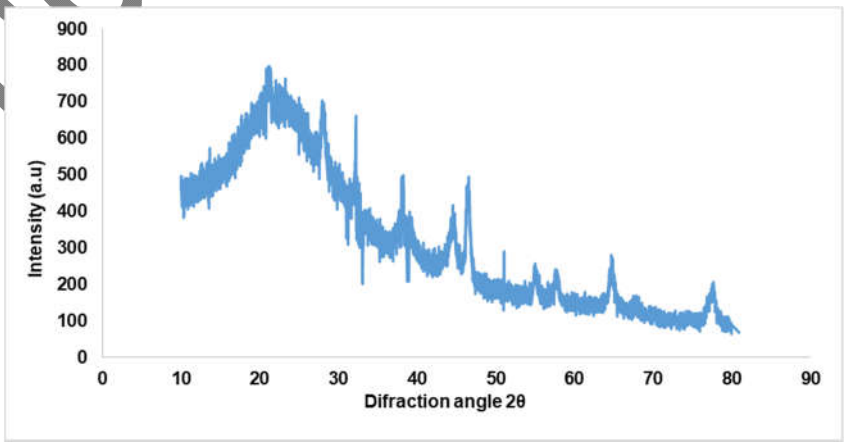

a)

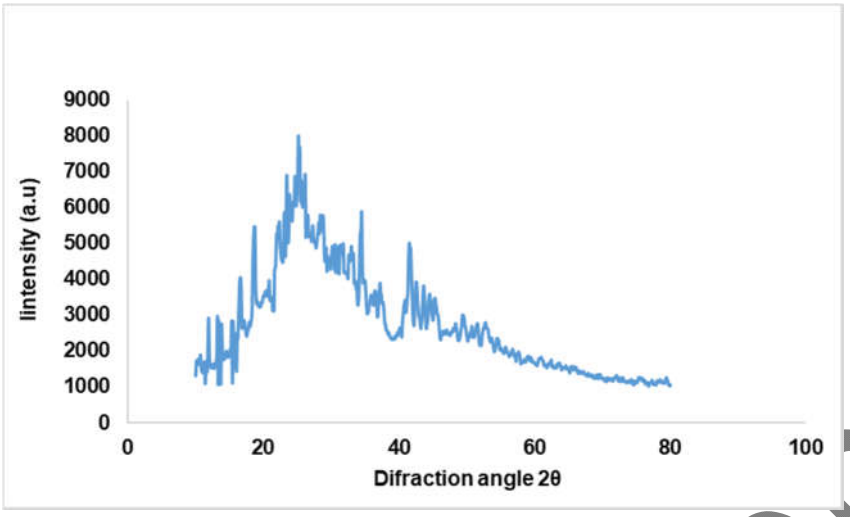

b)

Fig. 7: XRD images of (a) Dolutegravir (b) DF11

The XRD pattern shows a broad diffuse halo between 15°–35° (2θ) along with several small, irregular peaks, indicating that the material is mainly amorphous with very low crystallinity**.** The absence of sharp, intense diffraction peaks confirms a lack of long-range crystal order, suggesting that the sample is poorly crystalline or predominantly amorphous in nature.

Scanning electron microscopy

The Scanning Electron Microscopy (SEM) image of Dolutegravir reveals a heterogeneous mixture of particles with varying shapes and sizes, indicating a non-uniform surface morphology. The particles appear mostly irregular and aggregated, with sizes ranging from approximately 56.9 nm to 122.3 nm as marked in the image. The surface texture is rough, suggesting possible amorphous characteristics in line with the XRD results as per fig. 7. SEM image of DF11 reveals the morphological characteristics and particle size distribution of the sample. The observed structure consists of rod-shaped and irregularly shaped particles with varying sizes, indicating a heterogeneous distribution. The particle sizes range from approximately 136.2 nm to 275 nm**,** confirming nanoscale dimensions. The presence of agglomerates suggests possible particle interaction, which may influence the formulation's stability and performance. Overall, the SEM analysis provides critical insights into the microstructure and surface morphology of DF11, supporting its potential for intended pharmaceutical or material applications. The SEM image of pure Dolutegravir shows a heterogeneous mix of irregular, aggregated particles with rough surfaces, ranging from 56.9 to 122.3 nm, reflecting its amorphous nature as confirmed by XRD. The rough morphology may hinder solubility and bioavailability. In contrast, the optimized formulation DF11 exhibits a broader particle size distribution, ranging from 53.14 to 590.4 nm.

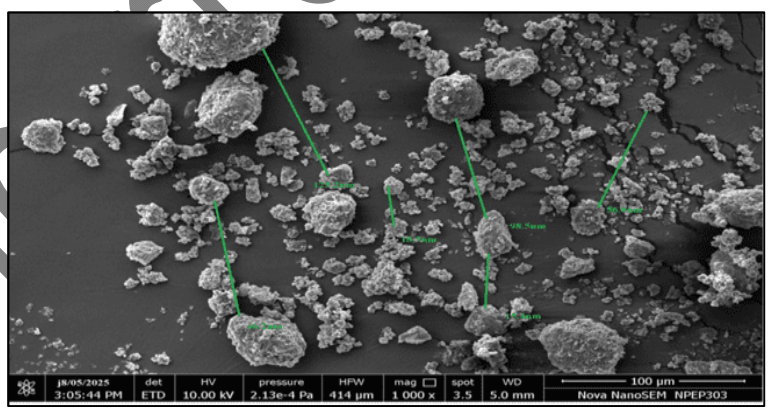

(a)

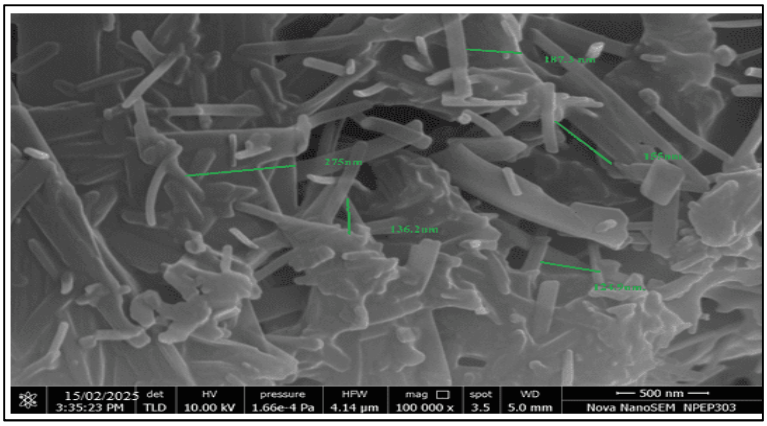

(b)

Fig. 8: SEM images of (a) Dolutegravir and (b) DF11

Stability study

The stability study of the optimized batch DF11 conducted over a period of three months demonstrated that the formulation remained physically and chemically stable. The drug content showed only a negligible decline from 97.53±0.001% at the initial point to 97.49±0.23%at the end of the third month, indicating no significant degradation of the API. The entrapment efficiency also exhibited minimal variation (from 93.92±0.02% to 93.85±0.03%), confirming that the drug remained securely encapsulated within the solid lipid matrix without leakage or structural disruption. A slight increase in the drug release was observed over the study period, rising from 95.02±0.01% initially to 95.97±0.38% at three months, which may be attributed to minor lipid relaxation or improved diffusion pathways during storage. Throughout the study, the physical appearance remained consistently milky, indicating the absence of aggregation, phase separation, or instability.

Table 10: Stability study of optimized batch DF11

Parameter	Initial	1	2	3
Drug Content (%)	97.53±0.001	97.52±0.002	97.51±0.14	97.49±0.23
Entrapment Efficiency (%)	93.92±0.02	93.89±0.03	93.86±0.12	93.85±0.03
Drug release (%)	95.02±0.01	95.01±0.02	95.95±0.23	95.97±0.38
Physical appearance	Milky type	Milky type	Milky type	Milky type

All values are expressed as mean±SD (n = 3).

The results in table 10 confirm that the DF11 formulation maintains its physicochemical integrity and therapeutic performance for at least three months. However, the present study does not specify whether stability evaluation was performed under accelerated conditions (40 °C/75% RH) or real-time conditions (25 °C/60% RH), which should be considered a limitation. Extended accelerated or long-term stability studies are recommended to establish the formulation's shelf life more comprehensively. Minor variation in drug content is acceptable within ICH stability guidelines (Q1A(R2). Entrapment efficiency stability indicates minimal structural disruption of lipid-based nanocarriers. Slight increase in drug release may occur due to lipid matrix relaxation during storage. Unchanged appearance suggests absence of instability phenomena such as aggregation or phase separation. Accelerated (40 °C/75% RH) and real-time (25 °C/60% RH) conditions are recommended as per ICH Q1A(R2) stability testing guidelines.

Pharmacokinetic study

The oral route of administration was studied in order to evaluate its r impact on Dolutegravir bioavailability and release profiles over 12 h. for the Dolutegravir API, DF2 and DF11 Batches. Non-compartmental analysis of Dolutegravir API, DF2 and DF11 was performed after extravascular administration using the linear trapezoidal method for AUC calculation. The concentration-AUC curves for Dolutegravir API, DF2 and DF11 are shown in fig. 9. After 12 h, the concentration of Dolutegravir API, DF2 and DF11 in the plasma was approximately 570.06 µg/ml, 587µg/ml and 552µg/ml respectively. So, DF11 formulation showing good bioavailability as compared to the Dolutegravir API, DF2. The results from the *in vivo* oral pharmacokinetic study showed a significant increase in AUC for DF11 and DF2. The AUC 0-t for DF11 was found to be higher as compared to the DF2 and API.

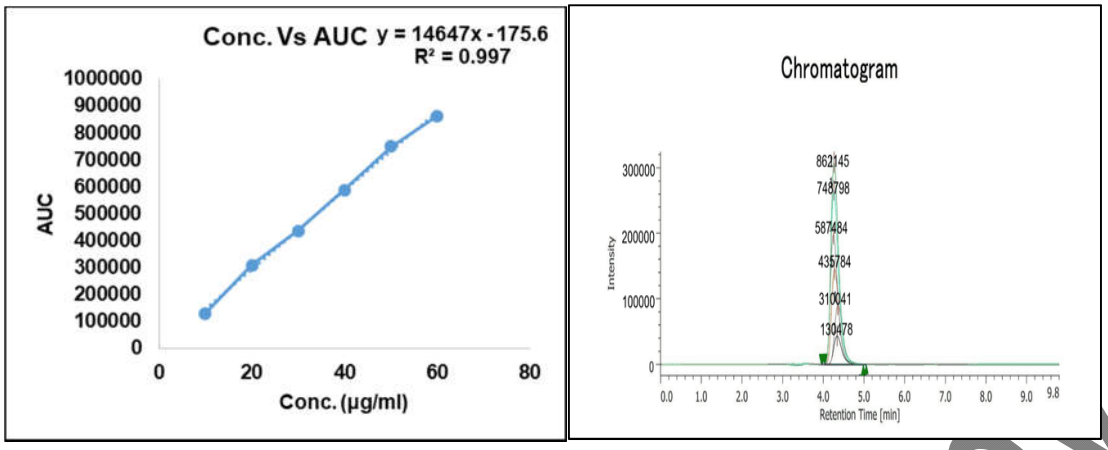

(a) **(b)**

Fig. 9: (a) Linearity graph of Dolutegravir and (b) HPLC chromatogram – linearity

Dolutegravir API

Dolutegravir exhibited a Cmax of 570.07 µg/ml at Tmax of 2 h with an elimination half-life ($t_1/_2$) of 6.5 h and MRT of 10.1 h. The AUC_0–∞ was 6228.14 µg·h/ml, indicating good systemic exposure, while apparent clearance (Cl/F) and volume of distribution (Vz/F) were 0.0040 (mg/kg)/(µg/ml)/h and 0.0376 (mg/kg)/(µg/ml)respectively.

Table 11: Summary table-input and output (Dolutegravir DF11)

Time	AUC	Conc.	Plasma drug conc.	ln(C)	AUC	AUMC	R^2	AdjustedR^2
0.15	14578	29225	166.42938	5.1145711	12.482204	1.8723306		
0.3	35684	50331	286.62301	5.6581678	46.461133	10.193679		
1	71454	86101	490.3246	6.1950676	318.3928	211.90271		
2	85457	100104	570.06834	6.3457562	848.58927	1027.1333	-0.9768343	0.9427565
3	71265	85912	489.24829	6.1928701	1378.2476	2331.0741	-0.968789	0.9180695
4	68745	83392	474.89749	6.163099	1860.3205	4014.7415	-0.9593046	0.8803981
6	55012	69659	396.69134	5.9831585	2731.9093	8294.4796	-0.922271	0.7011676
8	29854	44501	253.42255	5.5350583	3382.0232	12702.008		
12			205.56948	5.3257841	4300.0073	21690.436		

Dolutegravir DF11 Batch

Dolutegravir F1 formulation showed a Cmax of 587.14 µg/ml at Tmax of 2 h with a half-life of 5.94 h and MRT of 9.39 h. The AUC_0–∞ was 5701.05 µg·h/ml, and the apparent clearance (Cl/F) and volume of distribution (Vz/F) were 0.0044 (mg/kg)/(µg/ml)/h and 0.0376 (mg/kg)/(µg/ml), respectively.

Table 12: Summary table-input and output (Dolutegravir DF11)

Time	AUC	Conc.	Plasma drug conc.	ln(C)	AUC	AUMC	R	R_adj
0.15	11547	26194	149.16856	5.005077	11.187642	1.6781464		
0.3	29548	44195	251.67995	5.5281583	41.251281	9.0190917		
1	70215	84862	483.26879	6.180573	298.48334	204.58956		
2	88454	103101	587.13554	6.3752557	833.68551	1033.3595	-0.9729338	0.9332501
3	69855	84502	481.21868	6.1763218	1367.8626	2342.323	-0.9644608	0.9069127
4	62545	77192	439.58998	6.0858424	1828.2669	3943.331	-0.9490883	0.8511529
6	51454	66101	376.42938	5.9307305	2644.2863	7960.2672	-0.9040055	0.6344518
8	25474	40121	228.4795	5.4314465	3249.1952	12046.68		
12	18477	33124	188.63326	5.2398047	4083.4207	20229.55		

Dolutegravir DF2 Batch

Dolutegravir F2 formulation achieved a Cmax of 552.40 µg/ml at Tmax of 3 h with a half-life of 5.75 h and MRT of 9.22 h. The AUC_0–∞ was 6244.09 µg·h/ml, while the apparent clearance (Cl/F) and volume of distribution (Vz/F) were 0.0040 (mg/kg)/(µg/ml)/h and 0.0332 (mg/kg)/(µg/ml), respectively.

Table 13: Summary table-input and output (DF2)

Time	AUC	Conc.	Plasma drug conc.	ln (C)	AUC	AUMC	R	R_adj
0.15	17454	32101	182.80752	5.2084338	13.710564	2.0565846		
0.3	34545	49192	280.13667	5.6352776	48.431378	10.416244		
1	67541	82188	468.041	6.1485559	310.29356	203.64495		
2	76985	91632	521.82232	6.2573272	805.22523	959.48777		
3	82354	97001	552.39749	6.3142679	1342.3351	2309.9063	-0.9589593	0.892804
4	77154	91801	522.78474	6.2591698	1879.9263	4184.0721	-0.9492367	0.8515754
6	68544	83191	473.75285	6.1606858	2876.4638	9117.7281	-0.9143203	0.6719633
8	31547	46194	263.06378	5.5723965	3613.2805	14064.755		
12	21248	35895	204.41344	5.3201446	4548.2349	23179.698		

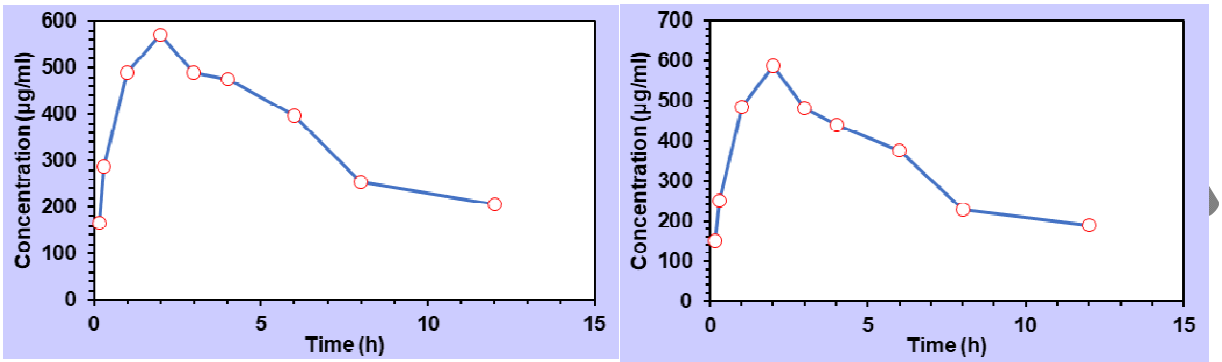

(a)(b)

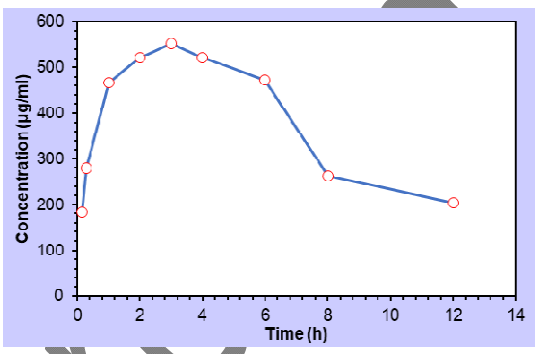

(b)

Fig. 10: Time in (min) Vs concentration (µg/ml) for (a) Dolutegravir API (b) DF11 batch (c) DF2 batch

DISCUSSION

The findings of the present study are in good agreement with previously reported investigations on antiretroviral drug-loaded solid lipid nanoparticles (SLNs). The optimized formulation (DF11) showed a nanosized particle range (~213 nm), high entrapment efficiency (>93%), and sustained drug release up to 12 h. Similar particle size ranges (200–400 nm) and high entrapment efficiencies have been reported for SLNs of antiretroviral drugs such as zidovudine, efavirenz, and dolutegravir, prepared using high-shear homogenization and ultrasonication techniques, confirming the suitability of this method for SLN preparation [15, 16].

Earlier studies have demonstrated that increased homogenization speed and surfactant concentration significantly influence particle size reduction and improve drug entrapment, which correlates well with the present study, where homogenization speed was identified as a statistically significant factor affecting drug content, entrapment efficiency, and drug release [10, 20].

The biphasic drug release pattern observed in the present study—characterized by an initial burst release followed by sustained release—is a typical characteristic of SLN systems and has been widely reported in the literature [4, 17]. The initial burst release may be attributed to drug adsorbed on or near the nanoparticle surface, whereas the sustained phase results from diffusion of drug entrapped within the solid lipid matrix [5, 18]. Such prolonged release behavior has been reported to improve therapeutic efficacy and reduce dosing frequency of antiretroviral drugs [3, 14].

The negative zeta potential value (–29.7 mV) obtained for DF11 is comparable with previously published SLN formulations and indicates good physical stability due to sufficient electrostatic repulsion between particles [9, 21]. Furthermore, the enhanced *in vivo* pharmacokinetic performance of DF11, reflected by increased AUC and prolonged plasma drug levels compared to pure dolutegravir, is consistent with earlier reports on SLN-based antiretroviral delivery systems [18, 22]. This improvement has been attributed to lymphatic uptake, reduced first-pass metabolism, and sustained drug release from lipid nanoparticles [7, 10].

Overall, comparison with previously reported studies clearly demonstrates that the present dolutegravir-loaded SLN formulation offers improved entrapment efficiency, controlled drug release, enhanced stability, and better oral bioavailability, thereby emphasizing the significance and relevance of the present work in the field of antiretroviral drug delivery [4, 15, 16].

CONCLUSION

The study successfully developed Solid Lipid Nanoparticles (SLNs) of Dolutegravir using high shear homogenization and ultrasonication techniques. Glyceryl monostearate and Poloxamer 188 were selected as the lipid and stabilizer, respectively, to achieve an optimized formulation. Among all batches, DF11 was identified as the best formulation with the smallest particle size (212.9 nm) and the lowest PDI (0.190), ensuring uniformity. Its highly negative zeta potential (–29.7 mV) confirmed good stability and resistance to aggregation. DF11 showed maximum drug content (97.53±0.001%) and entrapment efficiency (93.92±0.02%). *In vitro* drug release studies revealed a sustained release profile, achieving 95.02±0.01% release at 8 h. FTIR and DSC studies confirmed the compatibility of thedrug and excipients without chemical interactions. XRD and SEM analyses indicated a crystalline nature and smooth, uniform morphology of nanoparticles. Stability studies over three months confirmed minimal changes in drug content, entrapment efficiency, and release profile. Pharmacokinetic studies showed improved bioavailability of DF11 compared to the Pure drug, suggesting its potential for enhanced therapeutic efficacy and reduced dosing frequency.

FUNDING

Nil

AUTHORS CONTRIBUTIONS

Anita H. Pagar is the main author and contributed to the conception, design, literature review, data collection, and preparation of the manuscript. Ashish Y. Pawar contributed as the research guide and provided supervision, technical guidance, and critical revision of the manuscript. Santosh R. Tambe, Principal of MGV's College of Pharmacy, contributed by providing academic support and suitable content for the study.

CONFLICT OF INTERESTS

Declared none

REFERENCES

1. UNAIDS, Deeks SG, Lewin SR, Havlir DV. The end of AIDS: HIV infection as a chronic disease. World AIDS Day 2022: global HIV and AIDS statistics – fact sheet. Lancet. 2013. 2023. 2;382(9903):1525-33.
2. Sharma A, Jadhav S. Drug delivery strategies for improving the bioavailability of antiretroviral drugs. J Control Release. 2015;219:679-94.
3. Scioli Montoto S, Muraca G, Ruiz ME. Solid lipid nanoparticles for drug delivery: pharmacological and biopharmaceutical aspects. Front Mol Biosci. 2020;7:587997. doi: 10.3389/fmolb.2020.587997, PMID 33195435.
4. Dening TJ, Rao S, Thomas N, Prestidge CA. Novel nanostructured solid materials for modulating oral drug delivery from solid-state lipid-based drug delivery systems. AAPS J. 2016;18(1):23-40. doi: 10.1208/s12248-015-9824-7, PMID 26354801.
5. Doktorovova S, Souto EB. Nanostructured lipid carrier-based hydrogel formulations for drug delivery: a comprehensive review. Expert Opin Drug Deliv. 2009;6(2):165-76. doi: 10.1517/17425240802712590, PMID 19239388.
6. Pandey R, Sharma A, Zahoor A, Sharma S, Khuller GK, Prasad B. Poly (D,L-lactide-co-glycolide) nanoparticle-based inhalable sustained drug delivery system for experimental tuberculosis. J Antimicrob Chemother. 2003;52(6):981-6. doi: 10.1093/jac/dkg477, PMID 14613962.
7. Sanna V, Pala N, Sechi M. Targeted therapy using nanotechnology: focus on cancer. Int J Nanomedicine. 2014;9:467-83. doi: 10.2147/IJN.S36654, PMID 24531078.
8. . SC, . SV, . UU. Solid lipid nanoparticles: a review. JCPR. 2011;1(4):351-68. doi: 10.33786/JCPR.2011.v01i04.009.
9. Hou D, Xie C, Huang K, Zhu C. The production and characteristics of solid lipid nanoparticles (SLNs). Biomaterials. 2003;24(10):1781-5. doi: 10.1016/S0142-9612(02)00578-1, PMID 12593960.
10. Prabhakaran E, Hasan A, Karunanidhi P. Solid lipid nanoparticles: a review. Sci Rev Chem Comm. 2012;2:80-102.
11. Castelli F, Puglia C, Sarpietro MG, Rizza L, Bonina F. Characterization of indomethacin-loaded lipid nanoparticles by differential scanning calorimetry. Int J Pharm. 2005;304(1-2):231-8. doi: 10.1016/j.ijpharm.2005.08.011, PMID 16188405.
12. Padhye SG, Nagarsenker MS. Simvastatin solid lipid nanoparticles for oral delivery: formulation development and *in vivo* evaluation. Indian J Pharm Sci. 2013;75(5):591-8. PMID 24403661.
13. K S J, Sharma CP, Kalarikkal N, Sandeep K, Thomas S, Pothen LA. Evaluation of in-vitro cytotoxicity and cellular uptake efficiency of zidovudine-loaded solid lipid nanoparticles modified with Aloe Vera in glioma cells. Mater Sci Eng C Mater Biol Appl. 2016;66:40-50. doi: 10.1016/j.msec.2016.03.031, PMID 27207037.
14. Shaikh NA, Lala RR. Formulation development of dolutegravir sodium loaded nanolipid carriers for improved solubility and permeability. Int J Pharm Sci Res. 2021;12:3654-65.
15. Singh S, Dobhal AK, Jain A, Pandit JK, Chakraborty S. Formulation and evaluation of solid lipid nanoparticles of a water soluble drug: zidovudine. Chem Pharm Bull (Tokyo). 2010;58(5):650-5. doi: 10.1248/cpb.58.650, PMID 20460791.
16. Nachammai K, Nair KG, Velmurugan R, Pavithra KS. Sustained-release study on mefenamic acid and mosapride loaded solid lipid nanoparticles: *in vitro* characterization. Res J Pharm Technol. 2020;13(11):5391-8.
17. Manjunath K, Venkateswarlu V. Pharmacokinetics, tissue distribution and bioavailability of clozapine solid lipid nanoparticles after intravenous and intraduodenal administration. J Control Release. 2005;107(2):215-28. doi: 10.1016/j.jconrel.2005.06.006, PMID 16014318.
18. Kamarullah W, Indrajaya E, Emmanuella J. Potency of luteolin with solid lipid nanoparticle-PEG modification for artemisinin-resistant Plasmodium falciparum infection. Indones J Trop Infect Dis. 2018;7(3):80-5.
19. ALHaj NA, Abdullah R, Ibrahim S, Bustamam A. Tamoxifen drug loading solid lipid nanoparticles prepared by hot high pressure homogenization techniques. Am J Pharmacol Toxicol. 2008;3(3):219-24. doi: 10.3844/ajptsp.2008.219.224.
20. Shi F, Zhao JH, Liu Y, Wang Z, Zhang YT, Feng NP. Preparation and characterization of solid lipid nanoparticles loaded with frankincense and myrrh oil. Int J Nanomedicine. 2012;7:2033-43. doi: 10.2147/IJN.S30085, PMID 22619540.
21. Iqbal A, Zaman M, Wahab Amjad M, Adnan S, Abdul Ghafoor Raja M, Haider Rizvi SF et al. Solid lipid nanoparticles of mycophenolate mofetil: an attempt to control the release of an immunosuppressant. Int J Nanomedicine. 2020;15:5603-12. doi: 10.2147/IJN.S255636, PMID 32848390.
22. Babu VN, Rao GS, Budha RR, Alavala RR, Desu PK, Babu GK, et al. Development, characterization and optimization of solid lipid nanoparticles of alpha-mangostin by central composite design approach. J Appl Pharm Sci. 2023;13(8):140-50. doi: 10.7324/JAPS.2023.24237.
23. Mendoza-Muñoz N, Urbán-Morlán Z, Leyva-Gómez G, Zambrano-Zaragoza ML, Piñón-Segundo E, Quintanar-Guerrero D. Solid lipid nanoparticles: an approach to improve oral drug delivery. J Pharm Pharm Sci. 2021;24:509-32. doi: 10.18433/jpps31788, PMID 34644523.
24. Dudhat KR, V Patel H. Novel nanoparticulate systems for idiopathic pulmonary fibrosis: a review. Asian J Pharm Clin Res. 2020;13(11):3-11. doi: 10.22159/ajpcr.2020.v13i11.39035.